Electro-oxidation of ethanol in acid medium using carbon-supported PtRh nanoparticles with (100) preferential orientation

N.G. Pereira Filho, R.F.B. Souza, A.S. Ramos, R. M. Antoniassi, A. Oliveira Neto[*], *E. V. Spinacé*[*]

Instituto de Pesquisas Energéticas e Nucleares – IPEN-CNEN/SP, Av. Prof. Lineu Prestes, 2242, Cidade Universitária, 05508-900 São Paulo – SP, Brazil
[*]E-mail: espinace@yahoo.com.br; aolivei@ipen.br

Carbon-supported PtRh nanoparticles with preferential (100) orientation was prepared by an alcohol-reduction process using KBr as a shape directing agent. The electrocatalysts were characterized by EDX (energy-dispersive X-ray analysis), XRD (X-ray diffraction) and TEM (Transmission electron microscopy). The electro-oxidation of ethanol was studied by cyclic voltammetry and chronoamperometry at room temperature in acid medium. On-line differential mass spectrometry experiments were performed on a single cell of a direct ethanol fuel cell (DEFC) at 60 ^{0}C and the anodic effluents were analyzed by ATR-FTIR. PtRh/C (100) electrocatalyst showed cubic-like morphology and average nanoparticles size of 8 nm and provided superior DEFC performance (density power per Pt active area) and CO_2 selectivity compared to polycrystalline PtRh/C and commercial Pt/C electrocatalysts.

Keywords: PtRh nanoparticles; (100) preferential orientation, electrocatalysts; ethanol; fuel cell; DEFC

1. INTRODUCTION

A fuel cell converts chemical energy directly into electrical energy and among various types of fuel cells; Proton Exchange Membrane Fuel Cell (PEMFC) has received particular attention for potential implementation in portable, mobile and stationary applications [1, 2]. Hydrogen is the most fuel used in PEMFC and could be obtained from various sources (water, coal, methane, biomass) and using different processes (electrolysis and thermochemical processes) [2]. Thus, hydrogen is not a primary source of energy and it must be produced from other sources. Besides this, the hydrogen storage with a high mass/volume ratio at room temperature continues to be a challenge [3, 4]. In this manner, the use of

liquid fuels in PEMFC is very interesting principally for mobile applications due to the existing infrastructure [5]. Ethanol is attractive as a fuel because it can be produced in large quantities from biomass minimizing the production of greenhouse gases [6, 7]. However, it's complete oxidation to CO_2 still a challenge due the difficulty of C-C bond breaking of ethanol molecule and to the formation of CO intermediates that poison anode Pt electrocatalyts use in PEMFC [8, 9]. This result in acetaldehyde and acetic acid as the principal products formed for ethanol electro-oxidation in acid medium and only small quantities of CO_2 [8, 9]. It has been shown that the addition of small amounts of Rh to Pt catalysts improve the C-C bond breaking of ethanol molecule increasing the CO_2 formation [10-12]. In a previous work [13] a well-dispersed cubic Pt nanoparticles with preferential (100) orientation directly supported on carbon was prepared by a simple methodology (an alcohol-reduction process) using KBr as a shape-directing agent, which was easily removed by washing with water. The obtained Pt/C (100) electrocatalyst provided superior power densities and CO_2 selectivity for DEFC when compared to carbon-supported polycrystalline Pt nanoparticles. [13]. The synthesis of PtRh nanostructures with (100) preferential orientation has been described using organic compounds as shape-direct agents. Dai et al. [14] prepared PtRh supercrystal with (100) preferential orientation using N,N- dimethylformamide as the facet-specific agent of the (100) facets. Khi et al [15] synthesized facet-controlled dendritic nanostructures of (100)Rh–Pt using 1,2-hexadecanediol, stearic acid and octadecylamine. These materials showed nanoparticles sizes in the range of 30-50 nm. In this work, we prepared PtRh nanoparticles (average size of 8 nm) with preferential (100) orientation directly supported on carbon by a simple methodology using KBr as shape-directing agent [13] and employed as electrocatalyst for ethanol electro-oxidation in acid medium.

2. EXPERIMENTAL

2.1 Preparation of the electrocatalysts

2.1.1 Preparation of carbon-supported PtRh nanopartilces (PtRh/C eletrocatalyst)

PtRh/C electrocatalyst (20 wt% of metals and Pt:Rh atomic ratio of 95:5) was prepared by an alcohol-reduction process [13] by adding $H_2PtCl_6.6H_2O$ and $RhCl_3.3H_2O$ into an ethylene glycol:water (3:1, v:v) solution. The carbon support Vulcan XC 72R (Cabot Corporation) was added into this solution, which was submitted for 5 min in an ultrasonic bath. The resulting mixture was kept under reflux at 150 ^oC for 3 h before being filtered, washed with abundant water and dried for 5 h at 70^oC.

2.1.2 Preparation of carbon supported PtRh nanoparticles with preferential (100) orientation (PtRh/C (100) electrocatalyst)

PtRh/C (100) electrocatalyst (20 wt% of metals and Pt:Rh atomic ratio of 95:5) was prepared in the following way: Initially 30 wt% of the Pt precursor was added in a 50 mL round-botton flask containing 50 mL of an ethylene glycol/water solution (3/1, v/v) and 160 mg of Carbon Vulcan XC 72R

(Cabot Corporation). The round-botton flask was adapted with a reflux condenser and the mixture was heated under stirring until reaching the reflux temperature (~ 150 °C). After 15 min, an aqueous solution of KBr was added (Br⁻:Pt atomic ratio 300:1) and after 20 min a solution containing the remainder 70 wt% of the Pt precursor and 100 wt% of the Rh precursor (giving a final Pt:Rh atomic ratio of 95:5 and 20 wt% of metal loading) was added. The resulting mixture remained under reflux at 150°C for 145 min. Finally, the obtained solid was filtered, washed with abundant water and dried for 5 h at 70 °C.

2.2 Physico-chemical characterizations

The semiquantitative analysis of the electrocatalyst (metal wt% and Pt:Rh atomic ratios) were performed in a Philips Scanning Microscope, model XL30 with electron beam of 20 keV equipped with EDAX microanalyzer model DX-4.

X-ray diffraction analyses were performed using a Rigaku diffractometer model Miniflex II, using Cu Kα radiation source (λ = 0.15406 nm). The diffractograms were recorded in the range of 2θ between 20º and 90º with a step size of 0.05º and a scan time of 2 s per step.

TEM analysis were performed on a transmission electron microscopy (TEM –JEOL model JEM 2100, operating at 200 kV). The samples were prepared in the following way: an amount of the electrocatalyst was suspended in isopropyl alcohol and dropped in TEM cupper-grid coated with collodion film. The nanoparticles sizes were measured by end-to-end particle's extension.

2.3 Electrochemical performance

The electrocatalysts were electrochemically evaluated for ethanol electro-oxidation using cyclic voltammetry (VC) and chronoamperometry using a Metrohm Autolab PGSTAT 302N potentiostat/galvanostat. The experiments were conducted in a cell with three electrodes. As a counter electrode and reference electrode, a platinum wire and the reference hydrogen electrode (RHE) were used, respectively. As a working electrode, an electrode with an ultra-thin vitreous carbon layer with a diameter of 5 mm was used. The catalyst ink was prepared as follows: 10 mg of catalyst was dispersed in 1.8 ml of water, 1.2 ml of isopropyl alcohol and 50 μL of Nafion solution (5%). This ink remained for 30 min in the ultrasonic bath to ensure complete homogenization. 20 μL of this paint was deposited on the glassy carbon of the working electrode, dried with the aid of a heating lamp. As an electrolyte, a 0.5 mol L⁻¹ sulfuric acid solution was used and for the tests in the presence of fuel, a 1.0 mol L⁻¹ ethanol solution was used. Before and during the electrochemical experiments, ultrapure nitrogen was bubbled in order to remove the oxygen present in the electrolyte. For the CO stripping experiments, the working electrode was polarized at 0.25 V and carbon monoxide (CO) was bubbled into the electrolyte for 15 min, followed by nitrogen gas for 30 min. The scanning speed chosen for recording VCs was 50 mV s⁻¹, with all tests performed at room temperature. The current densities were normalized by the electrochemically active area of platinum, calculated from the cyclic voltamograms of each catalyst, using the following expression:

$$active\ area\ Pt = \frac{Q}{[Pt].qH}$$

where Q corresponds to the load referring to the integral of the hydrogen desorption area in the range of 0.05 - 0.4 V; [Pt] the mass of metal used (in mg) and qH the desorption load of a hydrogen monolayer on the platinum (210 µC cm^{-2}) [16].

2.4 On-line differential mass spectrometry experiments on single DEFC

The membrane electrode assemblies (MEA) were prepared by hot pressing a Nafion 117 membrane placed between commercial Pt/C, PtRh/C or PtRh/C (100) anode (1 mg Pt cm^{-2} catalyst loading) and a 20 wt% commercial Pt/C (Basf lot #F0381022) cathode (1 mg Pt cm^{-2} catalyst loading) at 125 $^{\circ}$C for 5 min under a pressure of 225 kgf cm^{-2}. The direct ethanol fuel cell performances were determined in a single cell with an area of 5 cm^2. The temperature was set to 60 ^{0}C for the fuel cell and 80 ^{0}C for the oxygen humidifier. The fuel was 2 mol L^{-1} ethanol solution delivered at approximately 1 mL min^{-1} and the oxygen flow was regulated at 300 mL min^{-1}. Polarization curves were obtained by using a potentiostat/galvanostat PGSTAT 302 N Autolab.

DEFC experiments were assisted by on-line differential mass spectroscopy (DMS) coupled to the anodic effluent output from the DEFC. The DMS setup consisted of two differentially pumped chambers and a quadrupole mass spectrometer, 200 a.m.u. DaQMS 200 M1, Prisma, Pfeiffer having a sensitivity of 200 A mbar^{-1}. The primary vacuum chamber was pumped with a rotary vane pump (DUO 5, Pfeiffer). The secondary chamber was pumped with a turbomolecular pump backed by a dry diaphragm pump (hicube 80, Pfeiffer). A gas-dosing valve (evn 116, Pfeiffer) connected the two chambers, and the DEFC/DMS interface was sitting on top of the primary vacuum chamber separated by a PTFE membrane (pore size 200nm Whatman®) in continuous flow, and monitored by multiple ion detection by QUADERA® software.

2.5 FTIR measurements

The aqueous effluents of the DEFC anodic compartment were collected for 600 seconds in vials at different increments of potential and analyzed by Attenuated Total Reflection-Fourier Transform Infrared (ATR-FTIR) using an ATR accessory (MIRacle with a ZnSe Crystal Plate Pike®) installed on a Nicolet® 6700 FT-IR spectrometer equipped with a MCT detector cooled with liquid N$_2$. Absorbance spectra were collected in the ratio (A:A$_0$) which A represents a spectrum at a given potential at the anode and A$_0$ is the spectrum obtained at ultrapure water.

3. RESULTS AND DISCUSSION

The polycrystalline PtRh/C electrocatalyst was prepared in a single step by the simultaneous reduction of Pt^{+4} and Rh^{+3} ions in the presence of carbon support forming polycrystalline PtRh nanoparticles supported on carbon. For the preparation of the PtRh/C (100) electrocatalyst, the procedure used was similar to that described for the preparation of the Pt/C (100) electrocatalyst [13]. Thus, a small

part of the Pt precursor was initially added for seed formation (small Pt nanoparticles), and after that, KBr was added to act as a shape-directing agent. Finally, when the solution containing the remainder of Pt^{+4} ions and Rh^{+3} ions was added, the reduction and grow on the formed seeds leads to the formation of PtRh nanoparticles with (100) preferential orientation directly supported on carbon.

The EDX analysis were performed in a semi-quantitative mode and the results are shown in Table 1.

Table 1. Chemical composition and Pt;Rh atomic ratios obtained by EDX (20 wt% and Pt:Rh atomic ratio of 95:5)

Electrocatalysts	Metal mass (wt %)	Pt:Rh (atomic ratio)
Commercial Pt/C	22	-
PtRh/C	23	95: 5
PtRh/C (100)	22	94.5: 5.5

For all electrocatalysts the metal loading (wt%) were similar to the nomimal ones and for PtRh electrocatalysts the Pt:Rh atomic ratio were very close to the nominal values. For PtRh/C (100) no KBr traces were not detected.
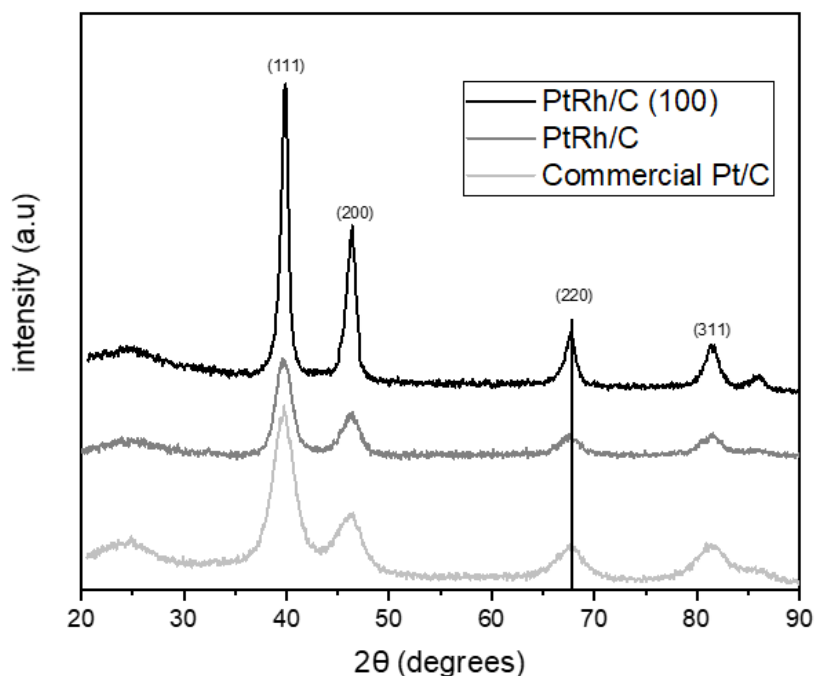

Figure 1. X-ray diffraction of the electrocatalysts

The X-ray diffractograms of the electrocatalysts are shown in Fig. 1. All diffractograms showed a broad peak at about 25° that was associated with the Vulcan XC72 support material and four peaks at approximately $2\theta = 40°$, 47°, 67°and 82°, which are associated with the (111), (200), (220) and (311)

Int. J. Electrochem. Sci., 16 **(2021)** Article Number: 211253

6

planes, respectively, of the face-centered cubic (fcc) structure characteristic of platinum and platinum alloys [13, 17]. In addition, it was observed that the peaks (220) of the electrocatalysts PtRh/C and PtRh/C (100), $2\theta \cong 67°$, presented a slight shift to lower angles, when compared with the peak of commercial Pt/C, inferring a possible formation of metallic alloy between Pt and Rh [17].

From the X-ray diffractograms, crystallite sizes were calculated from the Scherrer equation and the peak intensity ratios ($Pt_{(111)}/Pt_{(200)}$) were determined for the different electrocatalysts (Table 2).

Table 2. Crystallite sizes and peak intensity ratios ($Pt_{(111)}/Pt_{(200)}$)

Electrocatalysts	Crystallite size (nm)	Intensity ratio ($Pt_{(111)}/Pt_{(200)}$)
Commercial Pt/C	3	2.3
PtRh/C	3	2.3
PtRh/C (100)	8	1.5

The average crystallite size calculated for commercial Pt/C and PtRh/C electrocatalysts was 3 nm. For the material prepared with preferential orientation, PtRh/C (100), the crystallite size increase to 8 nm. The intensity ratios of the Pt(111)/Pt(200) peaks for commercial Pt/C and PtRh/C electrocatalysts were 2.3; while the electrocatalysts with Pt(100) surface domains exhibited the Pt(200) peak more intense and consequently the Pt(111)/Pt(200) intensity ratio of this material was lower (1.5). Similar results of average crystallite sizes and intensity ratios were already describe for polycrystalline Pt/C and Pt/C (100) electrocatalysts [13]. The transmission electron micrograph of PtRh/C (100) electrocatalyst and the histogram are shown in Fig. 2
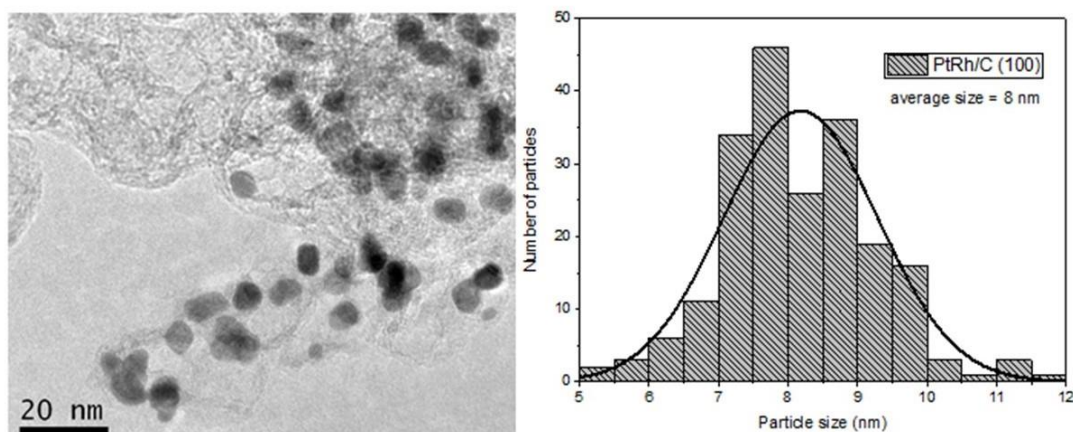

Figure 2. TEM image and histogram of PtRh/C (100) electrocatalyst

PtRh/C (100) electrocatalyst (Fig. 2) showed most of the nanoparticles having cubic-like morphology with a reasonable distribution on the carbon support and the histogram showed average nanoparticles size in range of 7-9 nm as already observed for Pt/C (100) electrocatalyst [13].

The voltammetric profiles for the electro-oxidation of carbon monoxide (CO-stripping) are shown in Fig. 3.
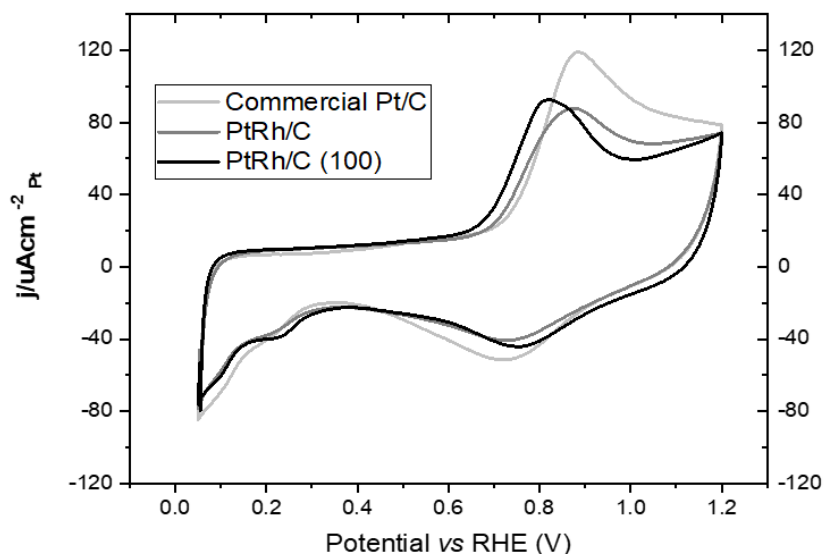

Figure 3. CO-stripping experiments of the electrocatalysts recorded at 50mVs^{-1} in 0.5 mol L^{-1} H$_2$SO$_4$

The CO stripping of the commercial Pt/C electrocatalyst showed only one peak of oxidation centered at approximately 0.87 V as reported in the literature for polycrystalline Pt/C electrocatalysts [18]. The voltammetric profiles of CO electro-oxidation of PtRh/C and PtRh/C (100) electrocatalysts, did not present relevant differences, showing only one peak of oxidation. However, for PtRh/C (100) electrocatalyst the peak occurred at approximately 0.80 V, while for the PtRh/C this peak occurred at 0.87 V. The CO oxidation on Pt terrace surfaces occurs at lower potentials, whereas in the edge and/or corner sites occur at higher potentials [19]. Thus, perhaps the lowest oxidation value observed for PtRh/C (100) electrocatalysts could be due to the increase of terrace surfaces resulting from cubic-like morphology of the nanoparticles.

The cyclic voltammograms of the electrocatalysts performed in acid medium are shown in Fig. 4. The cyclic voltamogram of Pt-based catalysts supported on carbon in an acid medium presents some characteristic peaks in the region of hydrogen desorption and adsorption (from 0.05 to 0.4 V), in the region of formation of the double electric layer (from 0.4 to 0.7 V), and in the region of formation of oxides (PtO$_x$), observed at potentials greater than 0.7 V. As each morphology has a concentration of different crystalline faces on the surface of the nanoparticles, the cyclic voltamograms exhibit different aspects in the first region of the graph (hydrogen desorption and adsorption). Thus, the cyclic voltamogram can provide information about the different crystallographic planes on the surface of the nanoparticles indicating their morphologies [13, 18].
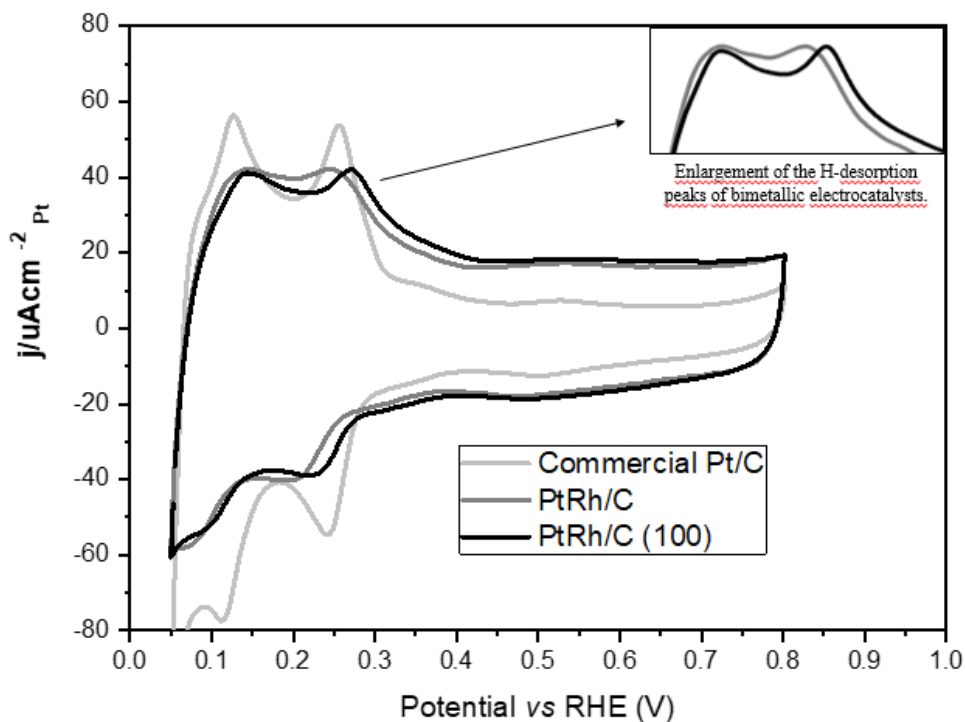
Figure 4. Cyclic voltammograms experiments of the electrocatalysts recorded at 50 mVs^{-1} in 0.5 mol L^{-1} H$_2$SO$_4$

Studies on hydrogen desorption in Pt monocrystals showed that the peak around 0.125 V corresponds to the process occurring at the Pt (110) sites, while the peak at approximately 0.27 V is associated with the process at the Pt (100) site, as well as approximately 0.34 to 0.37 V in the form of step and surface. Although it is in the region of the double electric layer, the peak $\cong$ 0.55 V is linked to the process at the Pt (111) sites [20]. It was observed for commercial Pt/C electrocatalyst that the Pt(110) peak is more intense than the Pt(100) resulting in an intensity ratio of I(100)/I(110) of approximately 0.94, which is characteristic of materials containing polycrystalline spherical nanoparticles [21]. For PtRh/C and PtRh/C (100) electrocatalysts it was observed that the hydrogen adsorption and desorption region is not as well defined as that of Pt electrocatalysts. This effect may be associated with the addition of Rh to Pt structure, as well as for carrying out experiments in an acid medium, where Rh has low electrocatalytic activity [22]. For PtRh/C electrocatalyst the peak of the Pt (110) sites had an intensity very close to the Pt (100), with the ratio between I(100)/I(110) being approximately 1.0. On the other hand, PtRh/C (100) electrocatalyst showed a slight increase in the intensity of the Pt (100) domain, with the I(100)/I(110) ratio being 1.03, which indicates a preferential growth on (100) plane. In addition, it was possible to observe a slight shoulder at approximately 0.37 V that was also described for Pt/C (100) electrocatalyst, but absent in polycrystalline electrocatalysts [13, 18].

Figure 5 showed the linear voltammograms of ethanol electro-oxidation and chroamperometry experiments at 0.5 V in ethanol solution with the current density values normalized per Pt active area.
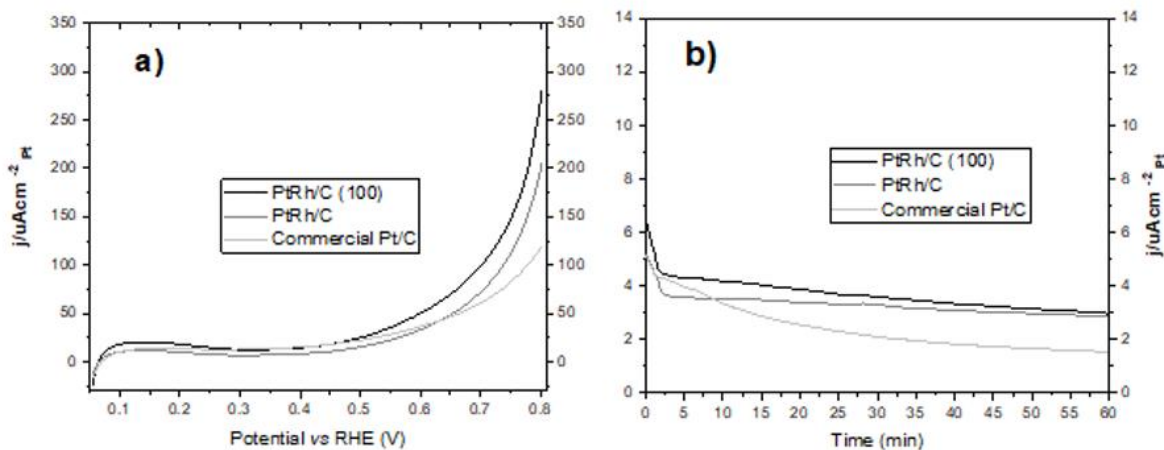
Figure 5. a) Linear Voltammograms and b) Chronoamperometry experiments at 0.5 V (0.5 mol L^{-1} of H$_2$SO$_4$ and 1.0 mol L^{-1} of ethanol)

It was observed for all electrocatalysts (Fig. 5 a) that the electro-oxidation of ethanol started at about 0.5 V and increase with the increase of the potential. PtRh/C (100) electrocatalyst showed higher current density values than commercial Pt/C and PtRh/C electrocatalyst in all potential range. In order to evaluate electrochemical activity and stability of the electrocatalysts, chronoamperometry experiments were performed at 0.5 V for 1 h (Fig. 5 b). In the first minutes of the experiments, a transient region was observed where there is a sharp drop in the values of current density for all electrocatalysts, being more pronounced for commercial Pt/C electrocatalyst. It was also observed throughout the experiment that PtRh/C and PtRh/C(100) electrocatalysts showed better density current values and good stability than commercial Pt/C.

DEFC experiments were performed with membrane electrode assemblies using the different electrocatalysts in the anode and commercial Pt/C in the cathode. The polarization curves are show in Fig 6.
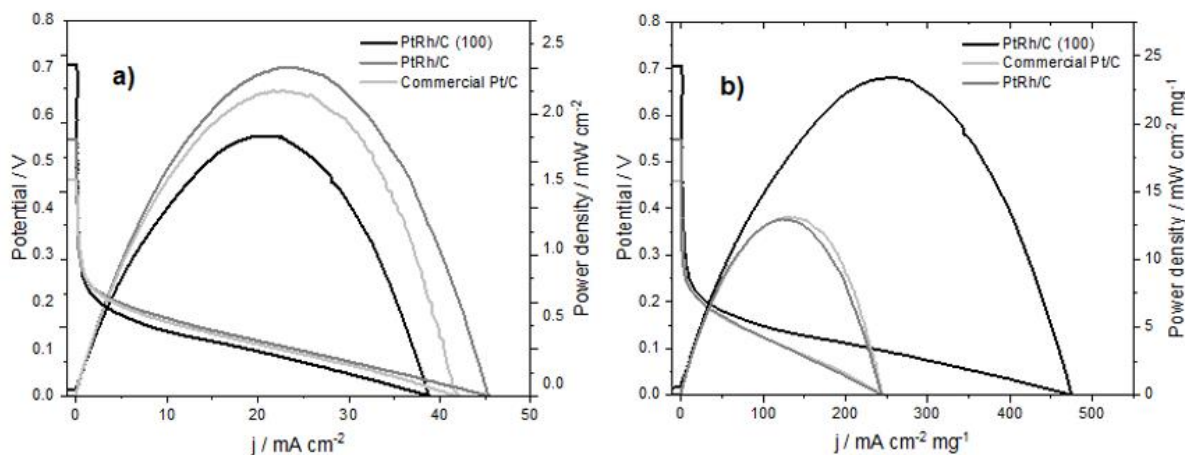

Figure 6. Power density curves for the different eletrocatalysts: a) normalized by electrode area and b) Pt active area

The polarization curves (Fig. 6) showed the following order for the open circuit voltage (OCV): PtRh/C (100) (0.7V) > PtRh/C (0.56 V) > commercial Pt/C (0.46 V). Evaluating the results of the electrical performance considering the MEA electrode area (Fig 6 a) the following order of performance was observed: PtRh/C > commercial Pt/C > PtRh/C (100). For comparative purposes, the power density values were also normalized by Pt active area of the electrocatalysts (Fig. 6 b) and, in this case, PtRh/C (100) electrocatalysts showed a significant increase of performance. This can be explained by the difference in the size of nanoparticles for the different electrocatalysts. While commercial Pt/C and PtRh/C electrocatalysts showed an average size of nanoparticles of around 3 nm; for PtRh/C (100) electrocatalyst this value increases to about 8 nm. This shows the importance of developing synthesis methodologies that allow obtaining nanoparticles with preferential orientation with smaller sizes. It is worth mentioning that PtRh/C(100) electrocatalyst showed a good electrical performance for both cases even presenting a larger nanoparticle size.

The DEFC electrical performance is a result of ethanol oxidation forming CO_2, acetaldehyde and acetic acid [23]. The anodic DEFC effluents using different electrocatalysts were analyzed on-line using differential mass spectrometry and the ion current of chemical species in function of potential values are shown in Figure 7. The possible chemical species formed from ethanol electro-oxidation show mass-to-charge ratio (m/z) of 44 that corresponding to CO_2 and/or acetaldehyde and m/z of 60 corresponding to acetic acid. Ethanol has m/z ratio of 46.
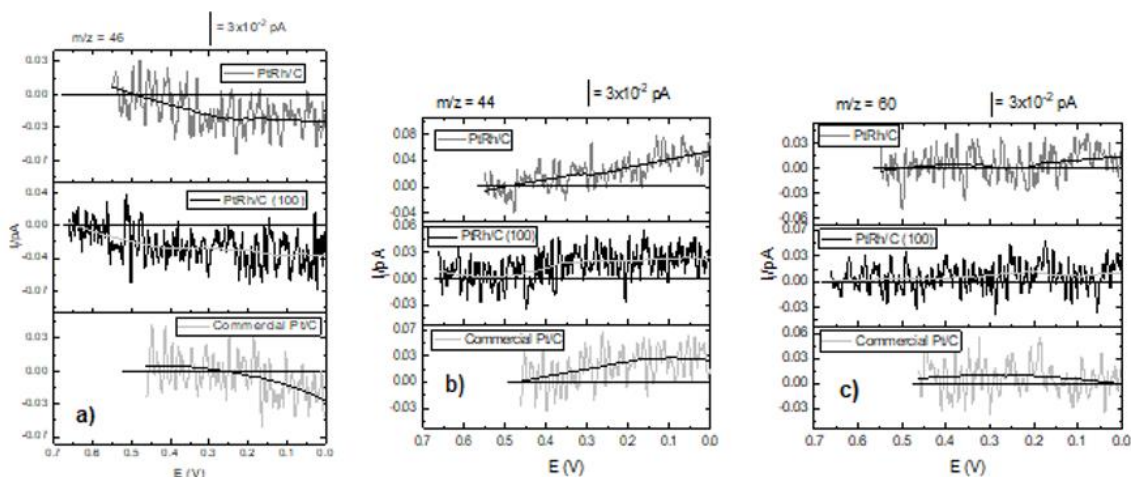

Figure 7. Ion current in function of potential values of the chemical species a) m/z = 46, b) m/z = 44 and c) m/z = 60 for different electrocatalysts

For the commercial Pt/C electrocatalyst (Fig 6 a) the ion signal intensity of m/z = 46 decrease from 0.2 V to 0 V, while for Pt/Rh/C electrocatalyst the ethanol consumption was observed between 0.5 and 0V and for PtRh/C (100) electrocatalyst between 0.65 V and 0V. For all cases, the ethanol consumption increased with the decrease of the potential. The variation of the ion signal intensity of m/z = 44 with the potential is shown in Fig.7b. This signal can be attributed to the formation of acetaldehyde and/or CO_2 and it was observed for commercial Pt/C electrocatalyst from near OCV (about 0.45 V) and

increased more significantly with decreasing potential to 0 V (maximum current density). PtRh/C electrocatalyst showed an increase of the ion signal intensity of m/z = 44 from 0.5 V and this increase grows almost linearly up to the potential of 0 V. PtRh/C (100) electrocatalyst also showed an increase of the ion signal intensity of m/z = 44 from 0.65V until 0.45 V and after that it remained practically constant until the potential of 0 V. The variation in the ion signal intensity of m/z = 60 confirmed the formation of acetic acid. For commercial Pt/C electrocatalyst this signal was observed from 0.45V and gradually decreased with decreasing potential to 0 V. For PtRh/C electrocatalyst the ion signal intensity of m/z = 60 was observed significantly only from 0.25 V and increased up to the 0 V potential. For PtRh/C (100) electrocatalyst the ion signal intensity of m/z = 60 is practically observed from 0.4 V and remained constant until the potential 0 V.

The DEFC anodic effluents collected at different potentials (V) were analyzed by ATR-FTIR and the spectra are shown in Figure 8.
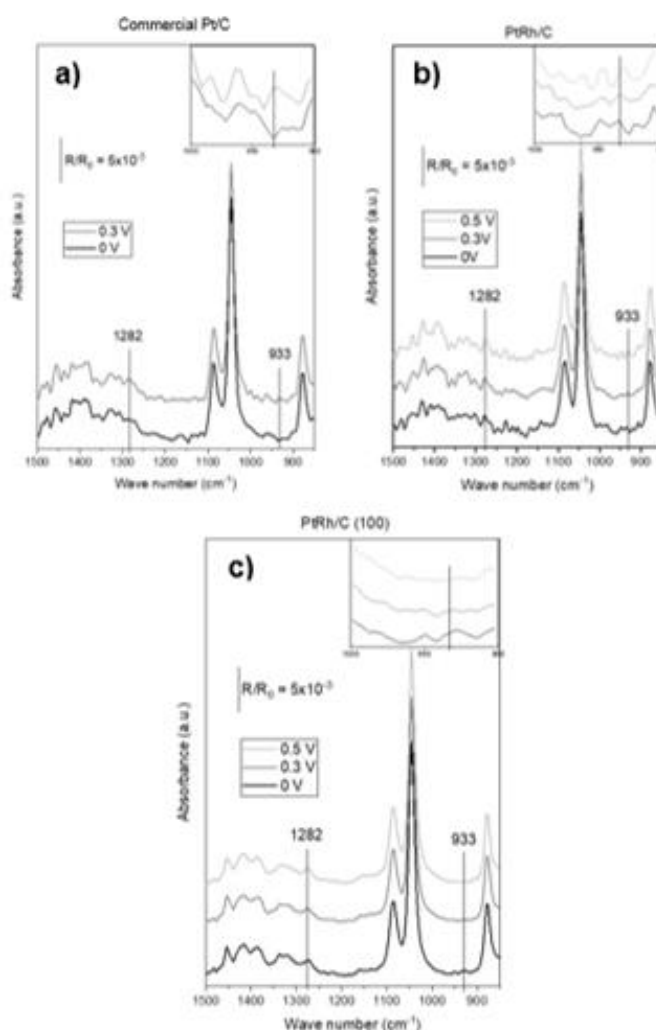

Figure 8. ATR-FTIR spectra of DEFC anodic effluents collected at different potentials

In the FTIR spectra the band at 1282 cm^{-1} was attributed to acetic acid and the band at 933 cm^{-1} to acetaldehyde [24]. The FTIR spectra of commercial Pt/C electrocatalyst showed the bands at 933 cm^{-}

[1] (acetaldehyde) and 1282 cm^{-1} (acetic acid) for the potential of 0.3 V; however these bands were no longer observable at 0 V suggesting that CO_2 was formed preferentially in high current regions. Thus, these results indicates a possible coexistence between acetic acid, CO_2 and acetaldehyde at potentials greater than 0 V and at potentials close to 0 V the formation CO_2 occurs preferentially over the formation of acetaldehyde. For PtRh/C electrocatalyst the bands at 933 cm^{-1} and 1282 cm^{-1} were observed for all samples collected at potentials between 0.5 and 0 V showing the coexistence of acetic acid, acetaldehyde and CO_2 as formed products throughout the potential range. For PtRh/C (100) electrocatalyst the band at 1282 cm^{-1} appears in all FTIR spectra recorded at different potentials, while the band at 933 cm^{-1} was more prominent for the sample collected at the potential of 0 V, indicating that CO_2 was preferably formed over the formation of acetaldehyde at the potentials between 0.5 and 0.3 V. Thus, these results suggest that PtRh/C (100) electrocatalyst provides a more complete oxidation of ethanol leading to the formation of acetic acid and CO_2 over a wider potential range.

4. CONCLUSIONS

Carbon-supported PtRh nanoparticles with preferential (100) orientation was prepared by a simple methodology using KBr as shape-directing agent. TEM images showed PtRh nanoparticles with cubic-like morphology and average size of 8 nm having a good dispersion on the carbon support. X-ray diffractogram showed a smaller (111)/(200) peak intensity and cyclic voltamogram in acid medium showed an increase in the intensity of the Pt(100) domain indicating a preferential growth on (100) plane when compared to polycrystalline PtRh/C and Pt/C electrocatalysts. Electrochemical experiments and DEFC tests also showed that PtRh/C (100) electrocatalyst was more active (per Pt active area) than PtRh/C and Pt/C electrocatalyst. On-line DMS experiments and ATR-FTIR measurements revealed that PtRh/C (100) electrocatalyst leads to the preferential formation of more oxidized products like acetic acid and CO_2 over a wider potential range compared to polycrystalline electrocatalysts.

References

1. S. J. Peighambardoust, S. Rowshanzamira, and M. Amjadi, *Int. J. Hydrogen Energy,* 35 (2010) 9349.
2. Y. Wang, D. F. Ruiz Diaz, K. S. Chen, Z. Wang and X. Cordobes Adroher, *Materials Today,* 32 (2020) 178.
3. I.Staffell, D. Scamman, A. Velazquez Abad, P. Balcombe, P. E. Dodds, P. Ekins, N. Shahd and K. R. Ward, *Energy Environ. Sci.*, 12 (2019) 463.
4. T. Q. Hua, H-S. Roh and R. K. Ahluwalia, *Int. J. Hydrogen Energy,* 42 (2017) 25212.
5. B. C. Ong, S. K. Kamarudin and S. Basri, *Int. J. Hydrogen Energy,* 42 (2017) 10142.
6. M. Z. F. Kamarudin, S. K. Kamarudina, M. S. Masdar and W. R. W. Daud, *Int. J. Hydrogen*

Energy, 38 (2013) 9438.
7.   S. P. S. Badwal, S. Giddey, A. Kulkarni, J. Goel and S. Basu, *Appl. Energy*, 145 (2015) 80.
8.   J. Bai, D. Liu, J. Yang and Y. Chen, *ChemSusChem.*, 12 (2019) 2117.
9.   M. A. F. Akhairi and S. K. Kamarudin, *Int. J. Hydrogen Energy,* 41 (2016) 4214.
10. P. Li, K. Liu, J. Ye, F. Xue, Y. Cheng, Z. Lyu, X. Liao, W. Wang, Q. Zhang, X. Chen, M. Liu and S. Xie, *J. Mater. Chem. A.*, 30 (2019) 17987.
11. Y. Zhu, L. Bu, Q. Shao and X. Huang, *ACS Catal.*, 9 (2019) 6607.
12. C. V. S. Almeida, D. S. Ferreira, H. Huang, A. C. Gaiotti, G. A. Camara, A. E. Russell, K. I. B. Eguiluza and G. R. Salazar-Banda, *Appl. Catal. B: Env.*, 254 (2019) 113.
13. R. M. Antoniassi, L. Otubo, J. M. Vaz, A. Oliveira Neto and E. V. Spinacé, *J. Catal.*, 342 (2016) 67.
14. L-X. Dai, X-Y. Wang, X-Y. Zheng and Y-W. Zhang, *Chem. Commun.*, 52 (2016) 5023.
15. N. T. Khi, J. Park, H. Baik, H. K. Lee, J-H. Sohn and K. Lee, *Nanoscale*, 7 (2015) 3941.
16. Y. Xing and M. Chen, *Langmuir*, 21 (2005) 9334.
17. S. S. Gupta and J. Datta, *J. Electroanal. Chem.*, 594 (2006) 65.
18. R. M. Antoniassi, J. C. M. Silva, T. Lopes, A. Oliveira Neto and E.V. Spinacé, *Int. J. Hydrogen Energy*, 42 (2017) 28786.
19. Y. Ye, J. Joo, S. Lee and J. Lee, *J. Mater. Chem. A.*, 2 (2014) 19239.
20. G. Tremiliosi Filho and V. P. dos Santos, *Quim. Nova*, 24 (2001) 856.
21. R. Devivaraprasad, M. Neergat, R. Ramesh, N. Naresh, T. Kar and R. K. Singh, *Langmuir*, 30 (2014) 8995.
22. M. Li, P.W. Zhou, N. S. Marinkovic, K. Sasaki and R. R. Adzic, *Electrochim. Acta*, 104 (2013) 454.
23. R. M. Antoniassi, A. Oliveira Neto, M. Linardi and E. V. Spinacé, *Int. J. Hydrogen Energy*, 38 (2013) 12069.
24. P. J. Linstrom and W. G. Mallard, *NIST Chemistry WebBook*, NIST Standard Reference Database Number 69. Available in: <https://webbook.nist.gov/chemistry/> Accessed in: 15 jun. 2021.
25. A.Kowal, M. Li, M. Shao, K. Sasaki, MB. Vukmirovic, J. Zhang, NS. Marinkovic, P. Liu, A.I. Frenkel and RR. Adzic, *Nat. Mater.,* 8 (2009) 325.
26. N. Erini, R. Loukrakpam, V. Petkov, E. A. Baranova, R. Yang, D. Teschner, Y. Huang, S. R. Brankovic and P. Strasser, *ACS Catal.*, 4 (2014) 1859.
27. G. Yang, A. I. Frenkel, D. Su and X. Teng, *ChemCatChem.*,8 (2016) 2876.